Three-Dimensional Full-Band Simulations of Si Nanowire Transistors

Mathieu Luisier, Andreas Schenk, and Wolfgang Fichtner
Integrated Systems Laboratory, ETH Zurich,
Gloriastrasse 35, 8092 Zurich, Switzerland; email: mluisier@iis.ee.ethz.ch

Abstract

In this paper the current characteristics of Si triple-gate nanowire transistors are simulated for different channel orientations. The full-band properties of Si are taken into account via the semi-empirical $sp^3d^5s^*$ tight-binding method. The three-dimensional electrostatic potential is solved self-consistently with the device charge density. This allows the treatment of more realistic transistor structures with rough semiconductor-oxide interfaces along the channel.

Introduction

Semiconductor nanowires are possible candidates to replace the actual metal-oxide field-effect transistors (MOSFET) since they can act both as active devices or as device connectors. Recently, with an individual nanowire, nanoscale field-effect transistors have been realized and reported in the literature [1]. As the active dimensions of these nanodevices are approaching the atomic scale, their transport properties must be treated on a quantum mechanical level.

Using the semi-empirical $sp^3d^5s^*$ nearest-neighbor tight-binding method [2], full-band (FB) simulations of Si triple-gate nanowire transistors are performed for different channel orientations such as [100], [110], and [111] in the ballistic regime. The three-dimensional (3D) electrostatic potential (Poisson's equation) is solved self-consistently with the FB transport calculation. Previous 'top-of-the-barrier' approaches [3] considered one-dimensional electrostatic potential only and semi-classical transport, but they gave a good insight into the device current characteristics. However their application is restricted to perfect atomic structures (no spatial variation of the nanowire cross section), whose energy dispersion ($E-k$) relation can be calculated. Our simulator furthermore includes short channel effects such as drain induced barrier lowering, tunneling through the barrier, lateral potential variation, and allows to treat Si-SiO_2 interface roughness at the nanowire surfaces. Energy relaxation of the atom positions is out of the scope of this paper. To emphasize the importance of full-band simulations, the current characteristics of a [100] channel-oriented wire are compared to effective mass (EM) calculations obtained by a three-dimensional coupled-mode space Non-Equilibrium Green's Function (NEGF) solver [4].

Approach

The $sp^3d^5s^*$ tight-binding bandstructure model is incorporated into a quantum transport solver via a new scattering boundary method [5]. Each nanowire is divided into slabs (wire unit cell, also called slice) of width Δ. The slabs are made out of atomic layers (all the atoms with the same x coordinate), whose number is related to the transport direction (4 for [100], 2 for [110], and 6 for [111]). In the 'top-of-the-barrier' approach all the slabs are identical, but with a 3D electrostatic potential the number of atoms per slab and the shape of a slab can vary along the nanowire channel.

Due to the very localized character of the Löwdin orbital functions used in the tight-binding method, electron charges $n(\mathbf{r})$ (holes are not considered in the simulations) and current densities $\mathbf{J}(\mathbf{r})$ are represented by δ functions centered around the atom positions $\mathbf{r_i}$ (bold letters stand for vectors)

$$n(\mathbf{r}) = \sum_i n_i \delta(\mathbf{r}-\mathbf{r_i}) \tag{1}$$

$$\mathbf{J}(\mathbf{r}) = \sum_{i,j} J_{ij}(\mathbf{r_j}-\mathbf{r_i})\delta(\mathbf{r}-\mathbf{r_i}). \tag{2}$$

n_i is the electron density at $\mathbf{r_i}$, J_{ij} is the current density flowing from one atom situated at $\mathbf{r_i}$ to its nearest neighbor at $\mathbf{r_j}$ (in principle four different j per i) along the bond connecting them.

To solve the three-dimensional Poisson equation without loosing the δ character of the carrier and the current densities, the finite element method (FEM) is chosen with a Delaunay grid. No atom is contained in the volume of any tetrahedron mesh element. Therefore the δ functions disappear when the electron density $n(\mathbf{r})$ is integrated with a test function.

The SiO_2 oxide layers do not participate to the transport calculation (only poor tight-binding representation available), but are included in the 3D electrostatic potential. Consequently, the oxide grid points carry no charge and hard wall boundary conditions are applied to the Si surface atoms. The nanowire roughness effects are generated by randomly distributing the atoms at the Si-SiO_2 interface according to an exponential autocovariance function [6].

Results

The upper part of Fig. 1 shows the schematic view of a triple-gate nanowire transistor of length $L_s+L_g+L_d \approx 32$ nm, composed of n-doped source and drain contacts (N_D=10^{20} cm^{-3}) and a three-part gate (top, left, and right). The Si channel of the transistor is a square of size 2.1 nm x 2.1 nm, whose transport direction x can be aligned with [100], [110], or [111], and which contains about 7300 atoms. The corresponding Si wire cross sections are presented in the lower part of Fig. 1 (only the [100] and the [110] cases). The

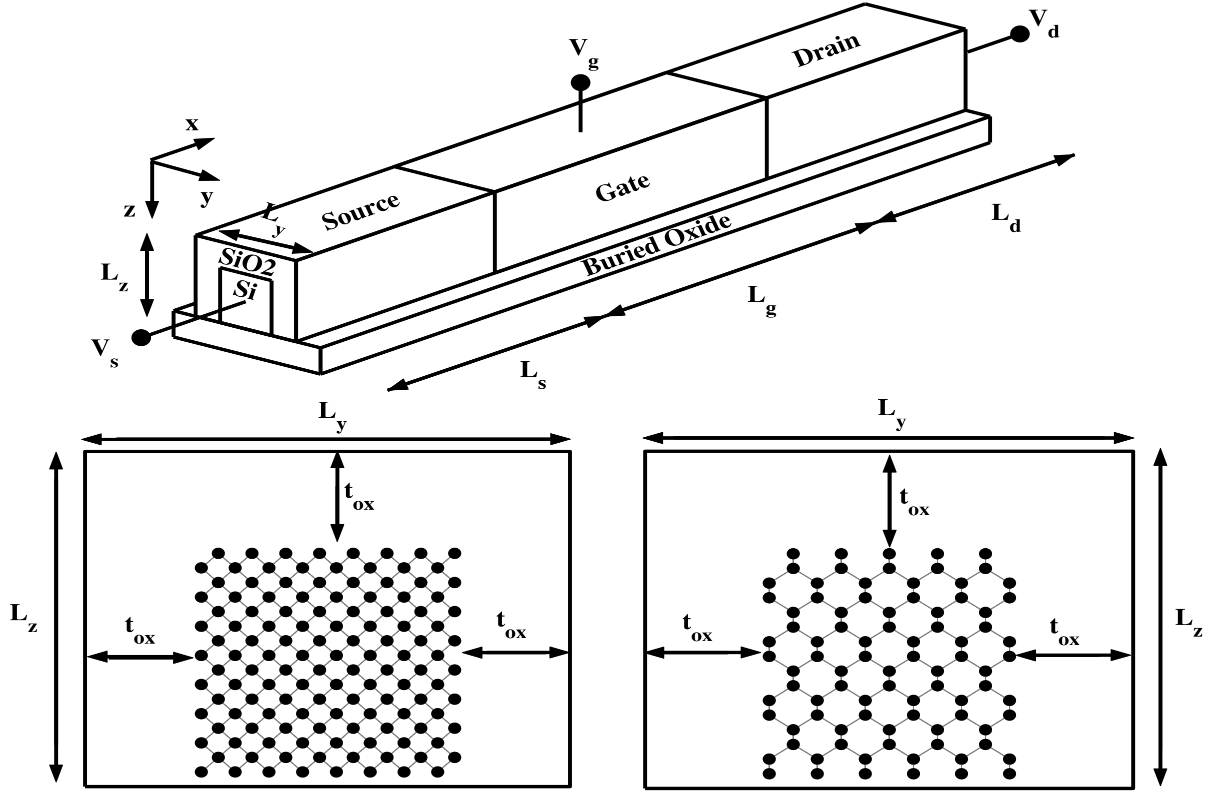

Fig. 1. Schematic view of a triple-gate Si nanowire transistor deposed on a buried oxide and surrounded by three oxide layers of thickness t_{ox}=1 nm. The source, the drain, and the gate measure L_s=10 nm, L_d=10nm, and L_g=12 nm, respectively. x is the transport direction, y and z are directions of confinement. The cross section of the nanotransistor (neglecting the buried oxide) has a size L_y=4.1 nm times L_z=3.1 nm. Two cross sections corresponding to different channel orientations are given in the lower part of the figure. Points represent Si atoms while lines model atomic bonds. The SiO_2 layers are not described in the tight-binding formalism. The nanowire channel (only Si atoms) is a 2.1 nm x 2.1 nm square. Left: transport along x=[100], 128 atoms per slab (Δ=0.543 nm), 60 slabs in the transistor. Right: transport along x=[110], 88 atoms per slab (Δ=0.384 nm), 84 slabs in the transistor. A potential V_g is applied to the gate (work funcion ϕ_m=4.25 eV), V_s to the source and V_d to the drain. The n-doped source and drain have a stoichiometric ratio f=2×10^{-3} of fully ionized donors.

[100] channel is composed of 60 slabs of width Δ=0.543 nm (transistor length=$60\times\Delta$=32.6 nm), each slab has 4 atomic layers and is made out of 128 atoms. For the [110] channel we count 84 slabs of width Δ=0.384 nm and 2 atomic layers with 88 atoms per slab. Finally the [111] channel contains 34 slabs (Δ=0.941 nm) with 6 atomic layers (210 atoms) per slab.

The full-band current characteristics of the different nanotransistors are depicted in Fig. 2. On the left, the FB (solid lines) and the EM (dashed lines) I_d-V_{ds} results are compared for a [100]-oriented channel and three different V_{gs} (0.5 V, 0.55 V, and 0.6 V). Due to the absence of non-parabolicity effects in the EM case, current channels turn on more slowly than in the FB case. This can be seen in Fig. 3, where the total transmission coefficient $T(E)$ from source to drain is plotted for V_{gs}=V_{ds}=0.4 V. The FB transmission (solid line) increases very fast (four channel in one step) while the EM transmission (dashed line) starts with two channels only. Consequently, the drain current I_d is underestimated by about 15% in the EM case.

On the right-hand side of Fig. 2, we simulate the 3D full-band $I_d - V_{gs}$ (V_{ds}=0.4 V) characteristics of the nanodevices with [100], [110], and [111] channel orientations. The comparison is done for the same gate metal work function ϕ_m=4.25 eV. This means that ϕ_m was not adjusted to obtain the same OFF-current ($I_{OFF} = I_d$ at V_{gs}=0 V and V_{ds}=0.4 V). As predicted by the 'top-of-the-barrier' approach [3], [110] (solid line with points) is the channel orientation that offers the highest drain current I_d at V_{gs}=V_{ds}=0.4 V, 9 times more than [100] (solid line) and 45 times more than [111] (solid line with circles). This is a consequence of the good compromise between the electron velocity (proportional to the inverse of the effective mass) and the number of available states (proportional to the effective mass) that is reached by the lowest conduction subbands in the [110] case. The lowest [111] conduction subbands, for example, have too heavy electrons that cannot flow efficiently from source to drain. The subthreshold swing S of the three nanowires is very close to its ideal value S=60 mV/decade.

Nanowires with a perfect crystal structure and a well-defined Si-SiO_2 interface will probably never be grown. The inclusion of the 3D electrostatic potential makes possible the

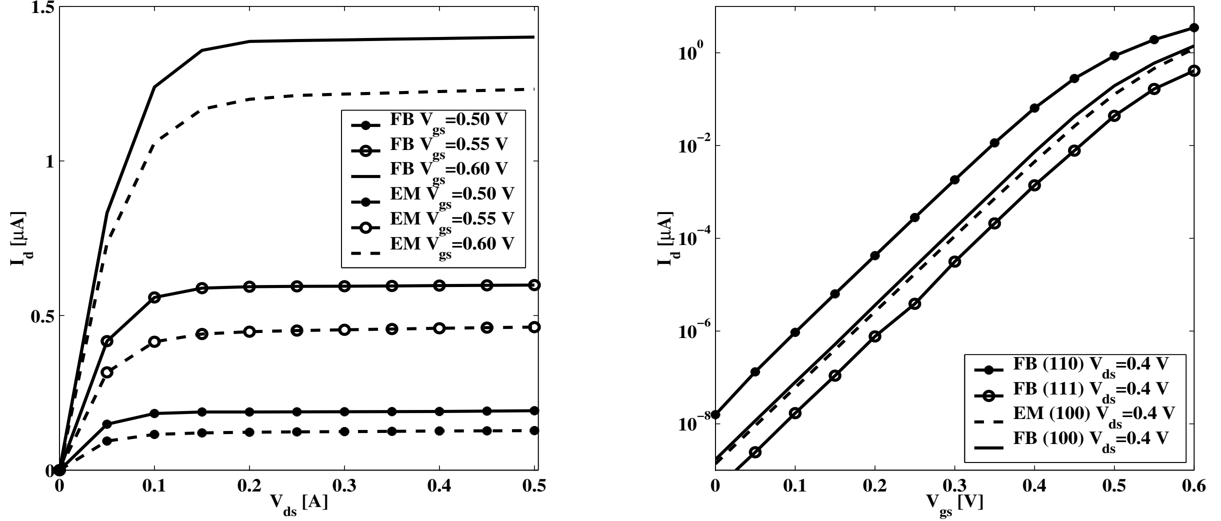

Fig. 2. Current characteristics of triple-gate nanowire transistors with different transport directions, calculated with a three-dimensional self-consistent electrostatic potential. The left subplot compares the $I_d - V_{ds}$ characteristics at three different V_{gs} for a [100] channel, obtained with full band (FB, solid lines) and with the effective mass approximation (EM, dashed lines). EM underestimates the current by 15% due to the absence of non-parabolicity effects in the bandstructure. The right subplot shows the $I_d - V_{gs}$ results at V_{ds}=0.4 V for transport directions x=[100] (FB: solid line, EM: dashed line), x=[110] (FB: solid line with points), and x=[111] (FB: solid line with circles). The highest drain current I_d at V_{gs}=V_{ds}=0.4 V is obtained for the [110] wire, as predicted by the 'top-of-the-barrier' ballistic FET model [3].

simulation of wires with a cross section (or slab contour) that varies from source to drain. The example of a non-ideal wire slab (channel orientation x=[100]), taken under the gate at the slab position 35 over 60, is given in Fig. 4. The atom positions in the middle of the slab are all occupied. At the Si-SiO_2 boundary some atoms are randomly removed others are added to form a rough interface.

Since all the nanowire slabs are different it is not possible to first construct a two-dimensional mesh with triangle elements on each slab and then to interpolate between the slab meshes to obtain tetrahedrons. A full 3D FEM mesh, as projected in Fig. 4, must be generated to calculate the electrostatic potential $V(\mathbf{r})$. Note that the mesh elements are finer around the atoms than in the oxide layers where $V(\mathbf{r})$ varies linearly due to the absence of charge.

In Fig. 5, the full-band $I_d - V_{gs}$ (V_{ds}=0.4 V) current characteristics of a structure with interface roughness (solid line) are compared to the results of an ideal structure (dashed line). For the simulated realization of the random Si-SiO_2 interface, the drain current I_d at V_{gs}=0.4 V is reduced to about 30% of its ideal value. However, another random distribution of the interface atoms will lead to a different I_d. The simulation of many nanowire samples yields an average $\tilde{I}_d$ at V_{gs}=0.4 V that is approximately 55% of the ideal drain current.

Current continuity is a very important property in the simulation of ballistic transistors. Interface roughness should not alter it. To demonstrate its validity the current I_d flowing from one nanowire slab to the other is reported in Fig. 6 for V_{ds}=0.4 V and for different V_{gs}. I_d is calculated in a non-ideal [100] nanowire by summing the current density contributions J_{ij} in Eq. (2) coming from all the bonds connecting two adjacent slabs.

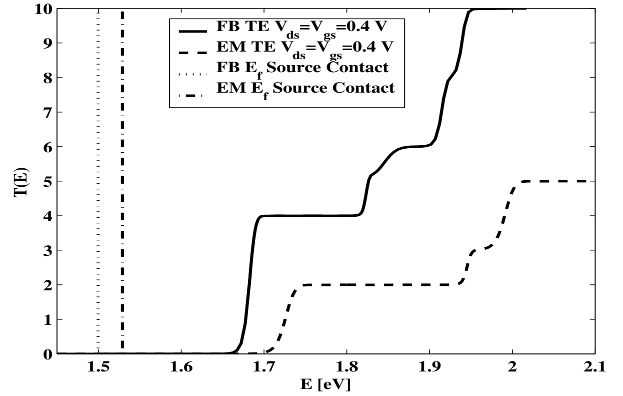

Fig. 3. Transmission coefficient T(E) through the [100] nanowire at V_{gs}=V_{ds}=0.4 V calculated with full band (FB: solid line) and with the effective mass approximation (EM: dashed line). T(E) in the FB case increases faster than in the EM case, leading to a larger drain current I_d. The vertical lines represent the source Fermi level with V_s=0 V.

Finally, Fig. 7 shows how interface roughness affects the electron distribution in the transistor. Because of the δ-character of the electron density $n(\mathbf{r})$, we can only plot the total number of electrons in each wire slab. The number of electrons per slab with interface roughness depends on three different effects: the electrostatic potential, the confinement of the y and z directions, and the conduction band edge lowering or increase caused by the modifications of the slab shapes.

Conclusion

In this paper, we presented the full-band simulations of ballistic Si nanowire transistors for different channel orientations.

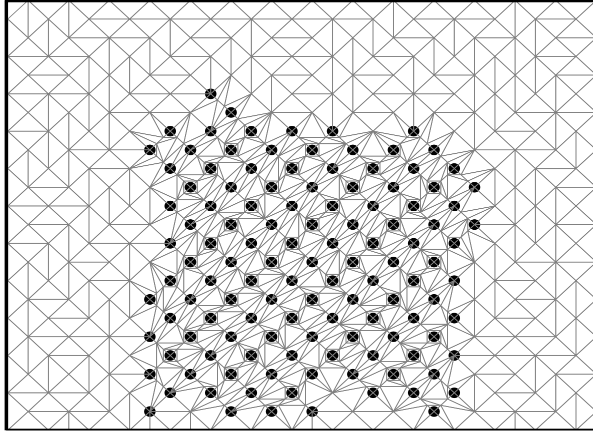

Fig. 4. Projection of the slab number 35 of the [100] nanowire transistor with interface roughness. Slab 35 includes 123 atoms instead of 128 as in the ideal case in Fig. 1. Bullets are Si atoms, lines represent the projection of the three-dimensional Delaunay finite element (FEM) mesh used to solve the self-consistent electrostatic potential.

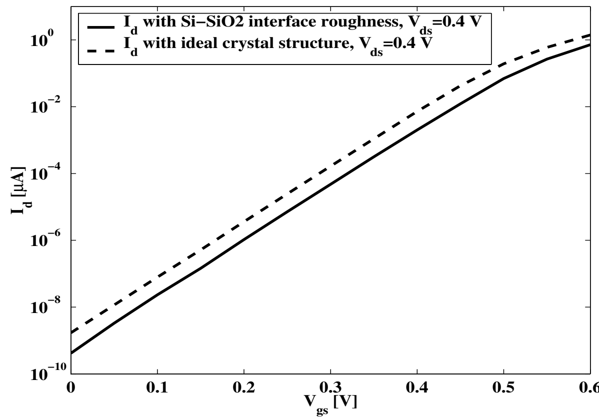

Fig. 5. Full-band current characteristics $I_d - V_{gs}$ at V_{ds}=0.4 V for a perfect [100] nanowire (dashed line) and for a [100] nanowire with Si-SiO$_2$ interface roughness. The drain current I_d at V_{gs}=V_{ds}=0.4 V is seriously deteriorated by the variation of the nanowire cross section. I_d with interface roughness represents only 30% of the ideal current. Such effects could not be observed with a 'top-of-the-barrier' approach [3].

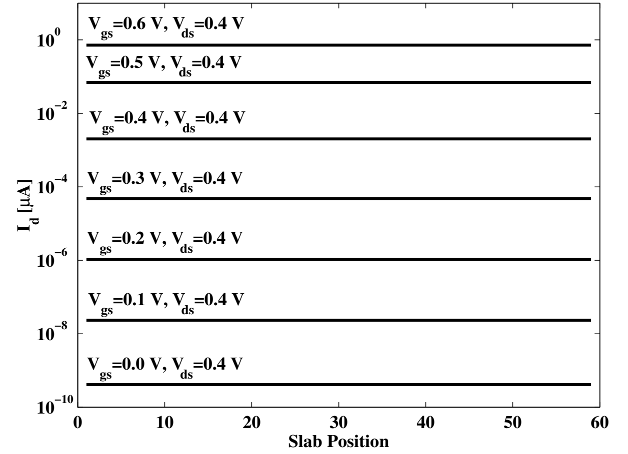

Fig. 6. Full-band current characteristics $I_d - V_{gs}$ at V_{ds}=0.4 V plotted along the [100] nanowire (60 slabs) with Si-SiO$_2$ interface roughness. Although the nanowire transistor is composed of slabs with different shapes and with a different number of atoms, the current is conserved in our approach.

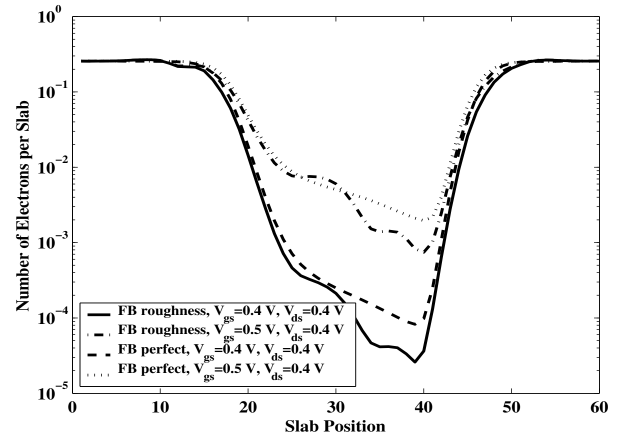

Fig. 7. Number of electrons per nanowire slab at V_{ds}=0.4 V and at two different V_{gs} for the [100] nanowire transistor. Two cases are depicted, both obtained with full-band (FB) transport solved self-consistently with the 3D electrostatic potential: a nanowire with an ideal structure (dashed and dotted lines) and a nanowire with Si-SiO$_2$ interface roughness (solid and dashed-dotted lines).

The results were obtained with the self-consistent coupling of the three-dimensional electrostatic potential and of the device charge density. New effects such as the atomic reconfiguration of semiconductor-oxide interfaces could be studied in this framework.

Acknowledgement

This work was supported by the Swiss National Fond (SNF), project 200021-109393 (NEQUATTRO).

References

[1] Y. Cui, Z. Zhong, D. Wang, J. Wang, and C. M. Lieber, *Nano Letters* 3, pp. 149-152, 2003.

[2] T. B. Boykin, G. Klimeck, and F. Oyafuso, *Phys. Rev. B 69*, p. 115201, 2004.

[3] J. Wang, A. Rahman, G. Klimeck, and M. Lundstrom, *IEDM Proc.* pp. 282-285, 2005.

[4] M. Luisier, A. Schenk, and W. Fichtner, *J. Appl. Phys.* 100, p. xxxxxx, 2006.

[5] M. Luisier, G. Klimeck, A. Schenk, and W. Fichtner, unpublished, 2006.

[6] S. M. Goodnick, D. K. Ferry, C. W. Wilmsen, Z. Liliental, D. Fathy, and O. L. Krivanek, *Phys. Rev. B* 32, pp. 8171-8186, 1985.